JOURNAL OF MATERIALS SCIENCE 15 (1980) 1663–1670

Fatigue striation in a wide range of crack propagation rates up to 70 μm/cycle in a ductile structural steel

C. MASUDA, A. OHTA, S. NISHIJIMA, E. SASAKI
Fatigue Testing Division, National Research Institute for Metals, 2–3–12, Nakameguro, Meguro-ku, Tokyo, Japan

The relationship between striation spacing and fatigue crack propagation rate up to 70 μm/cycle was investigated for a ductile structural steel, qualified as JIS SM58Q. A modified compact-type specimen 400 mm wide and a centre-cracked specimen 200 mm wide were tested at a stress ratio, R, of 0 and 0.8. The fracture surface of the specimen was examined in detail under a scanning electron microscope. The crack propagation rate was expressed by a power function of the range of stress intensity factor from 0.1 to 70 μm/cycle for $R = 0$ and to 0.5 μm/cycle for $R = 0.8$. The striation spacing coincided with the fatigue crack propagation rate over the range 0.1 to 70 μm/cycle. The profile of striation was found to be a "ridge and valley" type, and the ridges on one fracture surface coincided with those on the matching surface. It is suggested that the striation is formed by a plastic blunting mechanism.

1. Introduction

Fatigue crack propagation has usually been studied in one of the two ways, i.e., the application of linear fracture mechanics and the fractographic analysis of the fracture surface. The fatigue crack propagation rate, da/dN, is geneally expressed with a power function [1] of the range of stress intensity factor, ΔK, as

$$da/dN = C(\Delta K)^m \quad (1)$$

where C and m are constants obtainable by experiments. Equation 1 is known to be valid within the so-called intermediate region of da/dN (10^{-1} to 1 μm/cycle). A similar formula has been suggested by Miller [2] for the fatigue striation spacing, s, as

$$s = C_s(\Delta K)^{m_s}. \quad (2)$$

Several investigators have examined the relationship between da/dN and s, providing a possibility of practical applications in the failure analysis of structures. Fig. 1 shows a collection of published data for steels [3–6]. However, it is not clear if da/dN coincides with s in the higher and lower regions of da/dN (> 1 μm/cycle and < 0.1 μm/cycle, respectively).

Broek [7] examined the link between Equations 1 and 2 for two aluminium alloys and found that da/dN coincided with s only for values of da/dN from 0.1 to 1 μm/cycle. He explained that above this range da/dN was accelerated by the ductile fracture induced by intermetallic particles, while below the range, s became larger than da/dN because of inhomogeneous extension along the crack front. Is the situation the same in the case of structural steels, where we meet more frequently the necessity of quantitative analysis of accidental failures?

In the present work, the relationship between da/dN and s for wider range of da/dN values is studied. Large, modified compact-type specimens (W = 400 mm) were elaborated for this purpose, and tested under different stress ratios.

2. Experimental details

The material used in this study was a heat-treated high-strength steel, JIS SM58Q, generally used for welded structures. The material was maintained at 930° C for 1 h, and quenched in water, and then tempered at 650° C for 2 h. The chemical composition and mechanical properties are given in Table

0022–2461/80/071663–08$02.80/0

TABLE I Chemical composition of the material (%)

C	Si	Mn	S	P	Ni	Ni	Cr	V
0.14	0.32	1.30	0.006	0.022	0.024	0.20	0.023	0.038

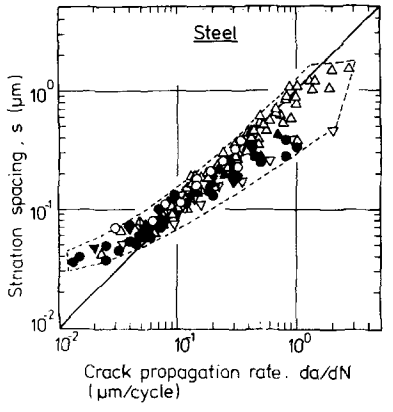

Material	Symbol	m	m_s	Reference
0.25%C Steel (A.C.)	○	2.7	2.2	[3]
0.55%C Steel (A.C.)	●	3.3	2.1	[5]
0.82%C Steel (700 F.C.)	●	3.1	2.1	[4]
0.82%C Steel (700 F.C., 25 h Ageing)	●	3.2	1.8	[4]
0.82%C Steel (850 F.)	●	4.0	2.1	[4]
0.35%C Steel (500 T.)	△	2.5	1.8	[5]
0.82%C Steel (400 T.)	▲	2.9	2.2	[4]
0.82%C Steel (600 T.)	▲	2.7	1.9	[4]
A 533 Steel (Grade B)	△	2.6	1.8	[6]
Ni–Cr–V Steel	△	2.0	1.3	[6]
HP9–4–25 Steel	△	1.9	1.6	[6]
Cr–Mo Steel (600 T.)	⧋	2.2	2.1	[3]
0.35%C Steel (200 T.)	▽	3.0	2.0	[5]
0.82%C Steel (250 T.)	▼	3.0	1.9	[4]
Cr–Mo Steel (300 T.)	▽	2.7	1.8	[3]

Figure 1 The relation between the crack propagation rate and striation spacing (data were collected from reports refered to in the figure).

I and II, respectively. The microstructure (Fig. 2) reveals an isotropic martensite of the material.

Fatigue tests were performed at two stress ratios, $R = 0$ and 0.8, on a 0.4 MN servo hydraulic testing machine, at 0.5 and 50 Hz in laboratory air. Two types of specimens, centre-cracked type (CC) and modified compact type (CT), were used in this study, as shown in Fig. 3. Both were sampled in such a way that the loading axis was in the longitudinal direction of the material.

The fatigue crack length was measured with a travelling microscope for CC specimens and with a crack follower for CT specimens.

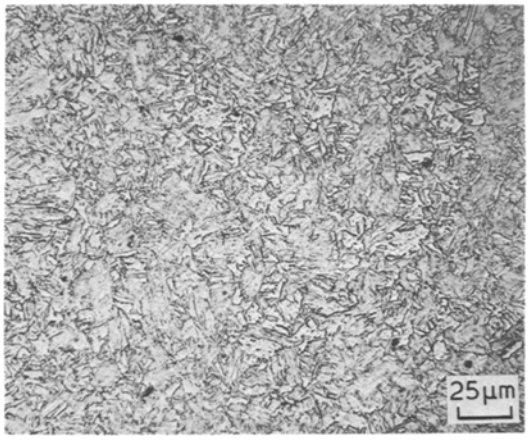

Figure 2 Microstructure of SM58Q steel.

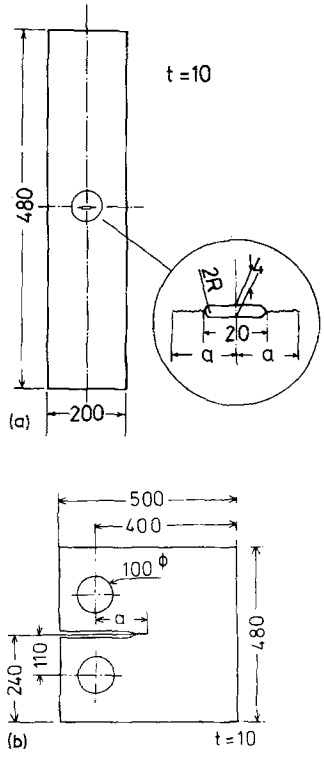

Figure 3 Fatigue test specimen. (a) Centre-cracked specimen (CC specimen). (b) Modified compact-type specimen (CT specimen).

TABLE II Mechanical properties of the material

σ_y (MPa)	σ_B (MPa)	δ (%)	H_v
590	670	27	230

ΔK-decreasing tests were performed for CC specimens in the lower da/dN region, while ΔK-increasing tests were carried out for CT specimens with a crack length increment of about 3 mm in the higher da/dN region.

The value of the stress intensity factor was calculated according to the following equations.

CC specimen [8]:

$$\Delta K = \frac{\Delta P\sqrt{a}}{BW}(1.77 + 0.227t - 0.51t^2 + 2.7t^3); \quad (3)$$

CT specimen [9]:

$$\Delta K = \frac{\Delta P}{BW} \cdot \frac{2+t}{(1-t)^{3/2}} \cdot (0.886 + 4.64t - 13.32t^2 + 14.72t^2 - 5.6t^4), \quad (4)$$

where ΔP is the load range, B the specimen thickness, W the specimen width, a the crack length, and $t = 2a/W$ for CC specimen or $t = a/W$ for CT specimen.

The fatigue fracture surface was examined at the mid-thickness of the specimens under a scanning electron microscope (SEM). Some stereographic observations were also carried out for discussing the mechanism of striation formation.

3. Experimental results

3.1. Fatigue crack propagation rate

The relationship between the range of stress intensity factor, ΔK, and the crack propagation rate, da/dN, was found in the present work as shown in Fig. 4. da/dN was measured on CC specimens for da/dN below 0.01 μm/cycle, while on CT specimens it was above that value. In the figure, the solid symbols indicate the points where the fracture surface was examined in the SEM.

It was found that the values of ΔK_{th}, the stress intensity threshold level, were above 7.9 MPa $m^{1/2}$ for $R = 0$, and 2.6 MPa $m^{1/2}$ for $R = 0.8$. Unstable fracture occurred at $\Delta K = 290$ MPa $m^{1/2}$ for $R = 0$, but at 58 MPa $m^{1/2}$ for $R = 0.8$.

It is evident for the material studied, that on log–log co-ordinates the crack propagation rate increases fairly linearly with increasing ΔK above

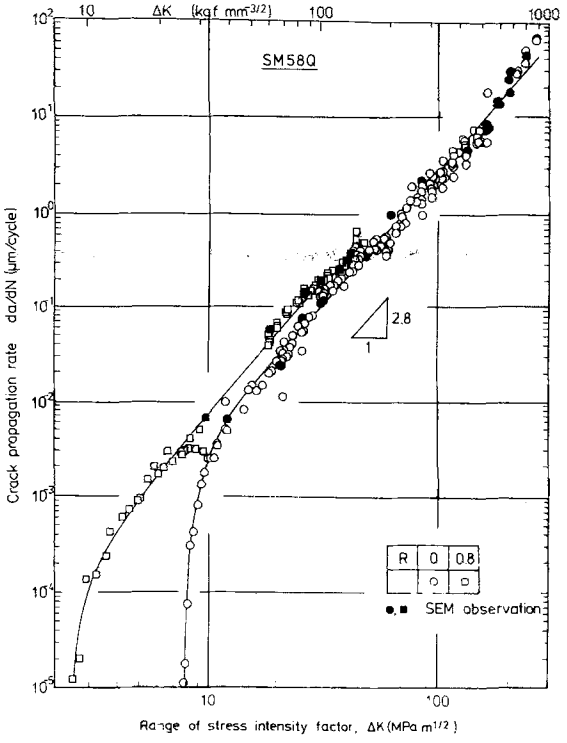

Figure 4 Variation of crack propagation rate with the range of stress intensity factor.

15 MPa $m^{1/2}$, and da/dN is generally larger for $R = 0.8$ than for $R = 0$ at given values of ΔK.

The exponent, m, in Equation 1 is about 2.8 for both stress ratios.

3.2. Fatigue microfractographs

Figs. 5 to 8 are examples of microfractographs taken at various da/dN values for $R = 0$ and 0.8. With the exception of Fig. 5, these are used for measurement of the striation spacing. Fig. 5 are lower magnification fractographs at the same spots of Fig. 6. These were taken in order to grasp the area fraction of the striation facet. In these microfractographs, the white arrows indicate the direction of microcrack propagation.

At very low rates of crack propagation, $da/dN = 0.007$ μm/cycle, the microstructure-sensitive facet was seen in most parts of the fracture surface, on the lower magnification microfractographs Fig. 5. This microstructure-sensitive facet corresponds to the martensitic structure shown in Fig. 2. The intergranular facet was not seen for the steel used in this study, although it has been observed in the low da/dN region for several steels [4, 10]. The striation spacing for $R = 0$ was nearly equal to that for $R = 0.8$ as shown in Fig. 6.

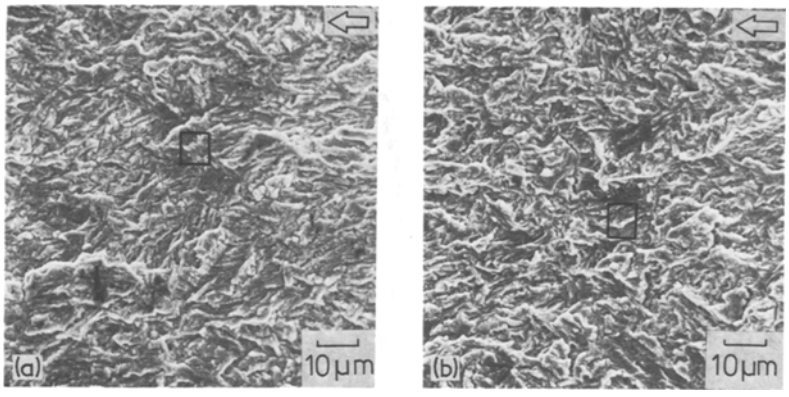

Figure 5 Lower magnification microfractographs observed at $da/dN = 0.007$ μm/cycle. (a) $R = 0$, $\Delta K = 12.4$ MPa $m^{1/2}$. (b) $R = 0.8$, $\Delta K = 9.9$ MPa $m^{1/2}$.

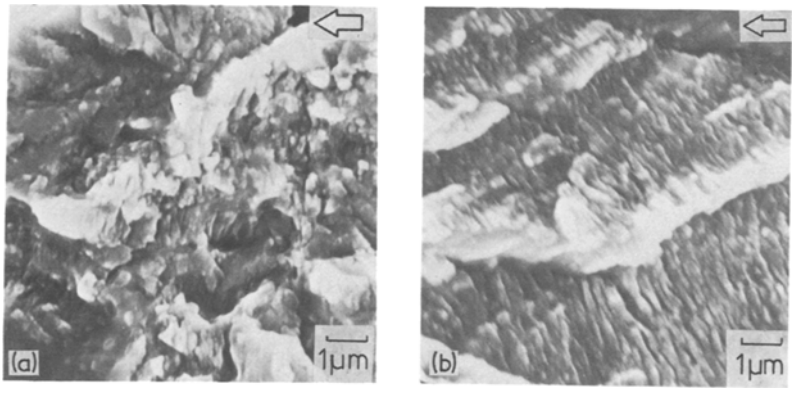

Figure 6 Higher magnification microfractographs of Fig. 5 observed at $da/dN = 0.007$ μm/cycle. (a) $R = 0$, $\Delta K = 12.4$ MPa $m^{1/2}$. (b) $R = 0.8$, $\Delta K = 9.9$ MPa $m^{1/2}$.

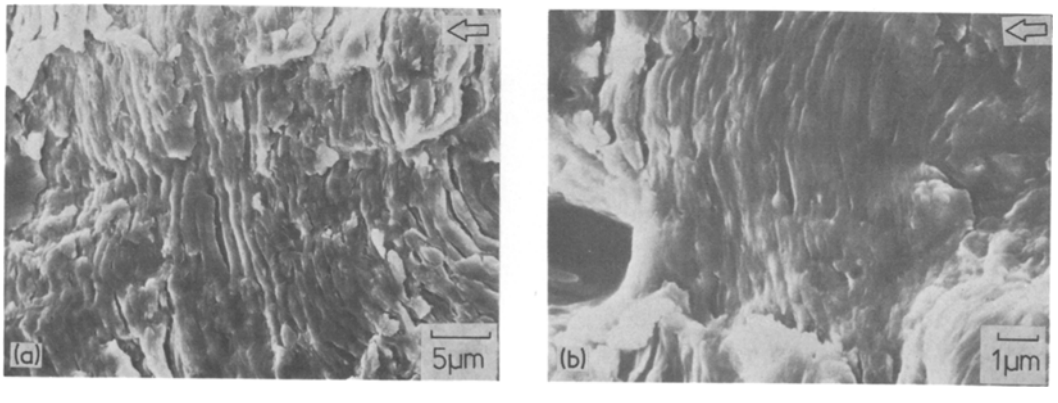

Figure 7 Microfractographs observed at $da/dN = 1$ μm/cycle. (a) $R = 0$, $\Delta K = 68.7$ MPa $m^{1/2}$. (b) $R = 0.8$, $\Delta K = 43.7$

At $da/dN = 0.1$ μm/cycle, the fracture surface aspect was principally the same as that observable for many ductile steels. The microstructure-sensitive facet disappeared, and the striation was observed on most of the fracture surfaces for $R = 0$ and 0.8. It consisted of fine striae parallel to each other and normal to the direction of crack propagation.

At $da/dN = 1$ μm/cycle (Fig. 7), the striation is always present on most fracture surface for $R = 0$

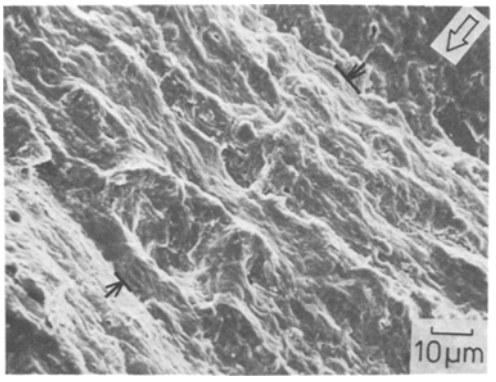

Figure 8 Microfractograph observed at $da/dN = 70$ μm/cycle for $R = 0$ at $\Delta K = 270$ MPa $m^{1/2}$.

and 0.8. Dimple and cleavage facets, frequently observed in this da/dN region for ductile steels [4, 5], were not found in this material.

For the very high range of propagation rate at $da/dN = 70$ μm/cycle (Fig. 8), the fracture surface was covered by striation markings parallel to each other and mixed with some dimples occupying a small fraction of the area. In the high range of da/dN for $R = 0.8$, stable crack growth was not observed. Therefore the microfractograph for $R = 0.8$ is not shown in Fig. 8.

3.3. Relationship between crack propagation rate and striation spacing

The striation spacing was determined as the average of about 100 striation markings counted on several microfractographs taken at different sites. The relationship between crack propagation rate and striation spacing is illustrated in Fig. 9. The straight line gives $s = da/dN$, and the region indicated by broken lines refers to the collected data shown in Fig. 1.

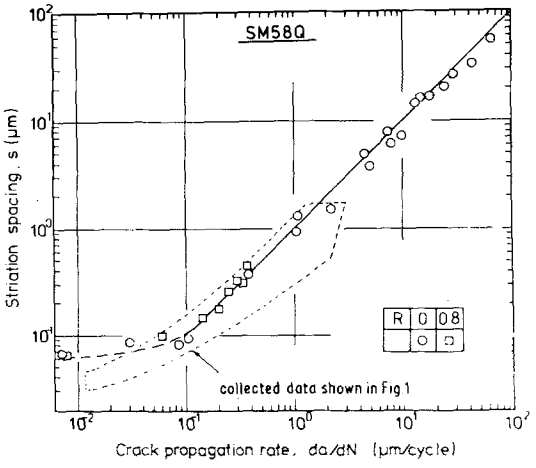

Figure 9 Relationship between crack propagation rate and striation spacing.

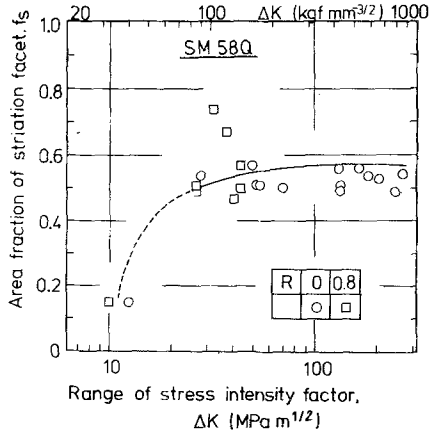

Figure 10 Variation of the area fraction of the striation facet with the range of stress intensity factor.

It is evident that the striation spacing is equivalent to the crack propagation rate for da/dN above 0.1 μm/cycle for $R = 0$ and 0.8. However, it is noted that the plots deviated upwards from the straight line for da/dN less than 0.1 μm/cycle.

3.4. Rating of striation facet

The relation between area fraction of striation facet, f_s, was determined according to the point counting method on lower magnification microfractographs such as Fig. 5. The relationship between f_s and ΔK is represented in Fig. 10. f_s was about 0.15 at very low ΔK values, and rapidly increased with increase of ΔK to attain a constant value of about 0.55 beyond $\Delta K = 30$ MPa $m^{1/2}$.

3.5. Stereo-matching observations

The striation profile was examined using a stereographic method with matching fractographic technique, mainly for the two points on the fracture surfaces corresponding to $da/dN = 0.007$ and 70 μm/cycle, respectively. Microfractographs were taken from three directions. The angles between the observed direction to the line normal to the fracture were $-15°$, $0°$, and $+15°$. Some typical results are given in Figs. 11 and 12. In these figures, the upper two views are those from the upper fracture surface, and the lower two from the matching lower one. The use of stereoviewer is indispensable to "read" these microfractographs.

From Fig. 11, reflecting the fracture at low da/dN, one can recognize that the patch Ⓒ on the lower fracture face, for example, shows a concavity, while the corresponding patch Ⓒ' on

Figure 11 Stereo-matching fractographs observed at $da/dN = 0.007$ μm/cycle.

the upper matching face presents a convexity. A similar irregularity is also found for the patches Ⓓ–Ⓓ′ in Fig. 12. Surface relief of this kind is generally compensating for two matching surfaces, and no systematic mismatch or cavity is observed between them.

As for the profile of striation marking, however, the situation is quite different. The fatigue striation shows a ridge and valley profile. The ridge is seen as the brighter parts in Figs. 11 and 12. Fig. 13 represents cross-sectional sketches of the striation profile. along line AA′ or BB′ defined in Figs. 11 and 12, respectively.

The ridge of the striation on the upper surface matches with that on the lower one. The front part of the ridge shows an inclined faced with a rumpled appearance consisting of wavy slip lines which are parallel to the ridge. It seems that the front part of the ridge is heavily deformed during the unloading part of the cycle.

Therefore, it is concluded that the striations both at 0.007 and 70 μm/cycle were also formed by a plastic blunting mechanism proposed by McMillan and Pelloux [11] in the intermediate da/dN region.

4. Discussions

The fatigue crack propagation rate, da/dN, coincides with the striation spacing, s, over the range 0.1 to 70 μm/cycle as in Fig. 9. In the same range, da/dN is well expressed by Equation 1 as stated in Section 3.1. These facts suggest that a single mechanism would govern the fatigue crack propagation over this range. The fractographic feature of Figs. 5 to 8, as well as the stereo-matching sketches in Fig. 13, support the above concept. Moreover, the area fraction of striation facet, f_s, in Fig. 10, remains nearly constant for ΔK above about 30 MPa $m^{1/2}$, or correspondingly $da/dN = 0.1$ μm/cycle. The reason for the difference between

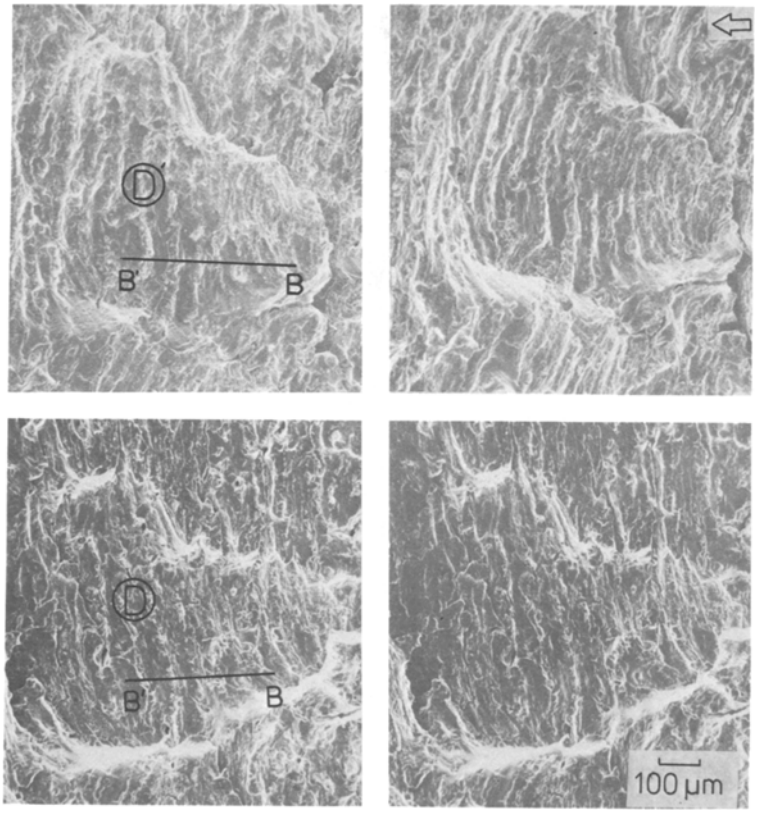

Figure 12 Stereo-matching fractographs at $da/dN = 70$ μm/cycle.

da/dN and s in the lower da/dN region seems to be the result of a small diminishing f_s in that region.

In Fig. 4, there is a difference between two stress ratios in the relationship between da/dN and ΔK. However, it should be considered that the same striation mechanism as the plastic blunting is the major controlling factor of fatigue crack propagation for both stress ratios, as discussed above. The concept of effective stress intensity range, ΔK_{eff}, proposed by Elber [12], is introduced here, in order to explain the results. The value of ΔK_{eff} means that the fatigue damage occurs only in the range which the crack tip opens. Measurement of ΔK_{eff} was performed using a displacement gauge mounted on a specimen surface straddling a crack far from the crack tip. The location of the displacement gauge has been recommended in a previous report [13]. After measurement of ΔK_{eff} using a displacement gauge, it was revealed that ΔK_{eff} has the same value for both stress ratios at the same value of da/dN. The linear relationship between da/dN and s for both ratios seems to result from the coincidence of ΔK_{eff} for both stress ratios.

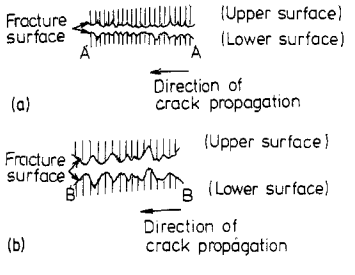

Figure 13 Sketch of the striation profile. (a) $da/dN = 0.007$ μm/cycle. (b) $da/dN = 79$ μm/cycle.

5. Conclusions

The fatigue crack propagation rate, da/dN, up to 70 μm/cycle was measured on large, modified compact-type specimens of width 400 mm under the stress ratios of 0 and 0.8 for ductile structural steel (JIS SM 58Q).

The fracture surface of the specimen was examined under a scanning microscope in order to reveal the striation mechanism. The relationship between da/dN and the striation spacing, s, was investigated. The following conclusions were obtained.

(1) The crack propagation rate is linearly related to ΔK, on log–log co-ordinates, up to the range of da/dN of 70 μm/cycle for $R = 0$ and of 0.5 μm/cycle for $R = 0.8$.

(2) The striations were observed over the range of $da/dN = 0.1$ to 70 μm/cycle.

(3) The cross-section of the striation shows a "ridge and valley" profile, and the ridge of the upper fracture surface coincides with that of the lower fracture surface.

(4) The striation spacing, s, coincides well with the fatigue crack propagation rate, da/dN, for da/dN larger that 0.1 μm/cycle.

(5) The area fraction of striation facet, f_s, tends towards a nearly constant value of about 0.5 over the value of $\Delta K > 30$ MPa $m^{1/2}$. f_s decreases with decreasing ΔK in the lower region.

Acknowledgements

The authors wish to thank Mr M. Shimodaira for his experimental work on the SEM, and Mr M. Kosuge for his experimental work on the measurement of the fatigue crack propagation.

References

1. P. C. PARIS and F. ERDORGAN, *Trans. ASME, J. Basic Eng.* **85** (1963) 528.
2. G. A. MILLER, *Trans. ASM* **61** (1968) 442.
3. C. MASUDA and S. NISHIJIMA, *Zairyo (J. Japan Soc. Mat. Soc.)* **27** (1978) 59.
4. Y. KISTUNAI, *Trans. Japan Soc. Mech. Eng.* **44–378** (1978) 385.
5. Y. KISTUNAI and M. TANAKA, *Preprints, Japan Soc. Mech. Eng.* **760–2** (1978) 35.
6. R. C. BATES and W. G. CLARK, JR, *Trans. ASM* **62** (1969) 380.
7. D. BROEK, "Proceeding of the 2nd International Conference on Fracture" (Chapman and Hall, London, 1969) p. 754.
8. W. F. BROWN, JR and J. E. SRAWLEY, ASTM STP 410 (1967) 11.
9. J. E. SRAWLEY, *Int. J. Fract.* **12** (1976) 475.
10. G. BERKBECK, A. INKEL and G. M. WALDRON, *J. Mater. Sci.* **6** (1971) 319.
11. J. C. McMILLAN and R. M. N. PELLOUX, ASTM STP 415 (1967) 505.
12. W. ELBER, ASTM STP 486 (1971) 230.
13. A. OHTA, M. KOSUGE, and E. SASAKI, *Int. J. Fract.* **15** (1979) R 53.

Received 21 August and accepted 13 November 1979.